Strong Spin-Orbit Coupling Effects on the Fermi Surface of Sr_2RuO_4 and Sr_2RhO_4

M. W. Haverkort,[1] I. S. Elfimov,[2] L. H. Tjeng,[1] G. A. Sawatzky,[2] and A. Damascelli[2]

[1]*II. Physikalisches Institut, Universität zu Köln, Zülpicher Straße 77, 50937 Köln, Germany*

[2]*Department of Physics and Astronomy, University of British Columbia, Vancouver, British Columbia, Canada V6T 1Z1*

(Received 29 February 2008; published 11 July 2008)

We present a first-principles study of spin-orbit coupling effects on the Fermi surface of Sr_2RuO_4 and Sr_2RhO_4. For nearly degenerate bands, spin-orbit coupling leads to a dramatic change of the Fermi surface with respect to nonrelativistic calculations; as evidenced by the comparison with experiments on Sr_2RhO_4, it cannot be disregarded. For Sr_2RuO_4, the Fermi surface modifications are more subtle but equally dramatic in the detail: Spin-orbit coupling induces a strong momentum dependence, normal to the RuO_2 planes, for both orbital and spin character of the low-energy electronic states. These findings have profound implications for the understanding of unconventional superconductivity in Sr_2RuO_4.

DOI: 10.1103/PhysRevLett.101.026406 PACS numbers: 71.18.+y, 74.70.Pq, 79.60.−i

The emergence of unconventional superconductivity in Sr_2RuO_4 from a rather conventional Fermi-liquid-like state has attracted the attention of numerous theoretical and experimental studies of this and related materials. Although Sr_2RuO_4 is isostructural with the high-T_c superconducting cuprates, there seems to be little doubt that the normal state is well described by a Fermi liquid, with a Fermi surface obtained from density-functional theory (DFT) band-structure calculations [1,2] which agrees well with experimental determinations. The Fermi surface of Sr_2RuO_4 has been measured with several techniques with an unprecedented accuracy: de Haas–van Alphen (dHvA [3]), Shubnikov–de Haas [4], low- and high-energy angle-resolved photoemission spectroscopy (ARPES [5,6]), and Compton scattering [7] data are all available for this compound and give a consistent outcome. The agreement of these experiments with calculations seems satisfactory, but it is not a trivial result, if one recalls the large many-body renormalization of the band dispersion [8] and the notion that Sr_2RuO_4 can be turned into a Mott insulator by Ca doping [9].

The apparent much weaker influence of electron correlation effects in the 4*d* ruthenates, as compared to the 3*d* cuprates, is not unexpected. The radial extent of the 4*d* wave functions with one radial node is much larger than the zero-node 3*d* one, leading to a larger one-electron bandwidth and a smaller on-site Coulomb repulsion. This fundamental difference between 3*d* and 4*d* transition metal compounds also explains the dominance of the t_{2g} band and low-spin-like behavior in describing the low-energy scale physics for systems with less than 6*d* electrons. In other words, Hund's rule splittings are eclipsed by crystal-field and band-structure effects in 4*d* systems. All of this would suggest that Sr_2RhO_4, with one extra 4*d*-t_{2g} electron, should also be well described by band theory and could provide an interesting approach to study the behavior of the unconventional superconducting state of Sr_2RuO_4 upon electron doping. Although one does expect the Fermi surface to change with the addition of one extra electron to the Fermi sea, it came as a surprise that band theory—within an approach equivalent to that used for Sr_2RuO_4—failed badly in describing the Fermi surface of Sr_2RhO_4, as determined to a high degree of precision by both ARPES [10,11] and dHvA experiments [12].

The subject of this Letter is to understand the reason for this discrepancy. It has been suggested that the failure of DFT in the case of Sr_2RhO_4 is a consequence of many-body interactions [10,11]. This seems, however, an unlikely scenario since, on general grounds, many-body effects are expected to be of the same magnitude in Sr_2RhO_4 and Sr_2RuO_4. Indeed, as confirmed by experimental determinations of mass enhancement [3,10] and quasiparticle dispersion [8,10], the renormalization parameters are closely comparable for the two compounds and, at most, would suggest slightly larger renormalization effects for Sr_2RuO_4. We will show that electron correlations are not the main driving force here; instead, the problem can be well understood by taking into account the interplay between spin-orbit coupling (SOC) and the details of the band dispersion close to the Fermi energy. In addition, the inclusion of SOC leads to a nontrivial, hitherto unknown, momentum dependence for orbital and spin characteristics of the near-E_F electronic states in Sr_2RuO_4; their knowledge is at the very heart of the microscopic understanding of spin-triplet, possibly orbital-dependent, superconductivity [13].

Experimentally, it was shown that SOC does play an important role in insulating ruthenates [14]. This is not surprising since the atomic relativistic SOC constant is $\zeta =$ 161 (191) meV for Ru^{4+} (Rh^{4+}) [15], which is not a small quantity. Furthermore, it is also rather similar for the two systems, leading one to believe that, if SOC is not important for the metallic ruthenates, the same should hold for the rhodates and vice versa. As we will show, the inclusion of SOC dramatically improves the agreement between DFT and experimental results for Sr_2RhO_4; we will also explain why SOC has a much smaller apparent effect for Sr_2RuO_4. Care should be taken, however, since for

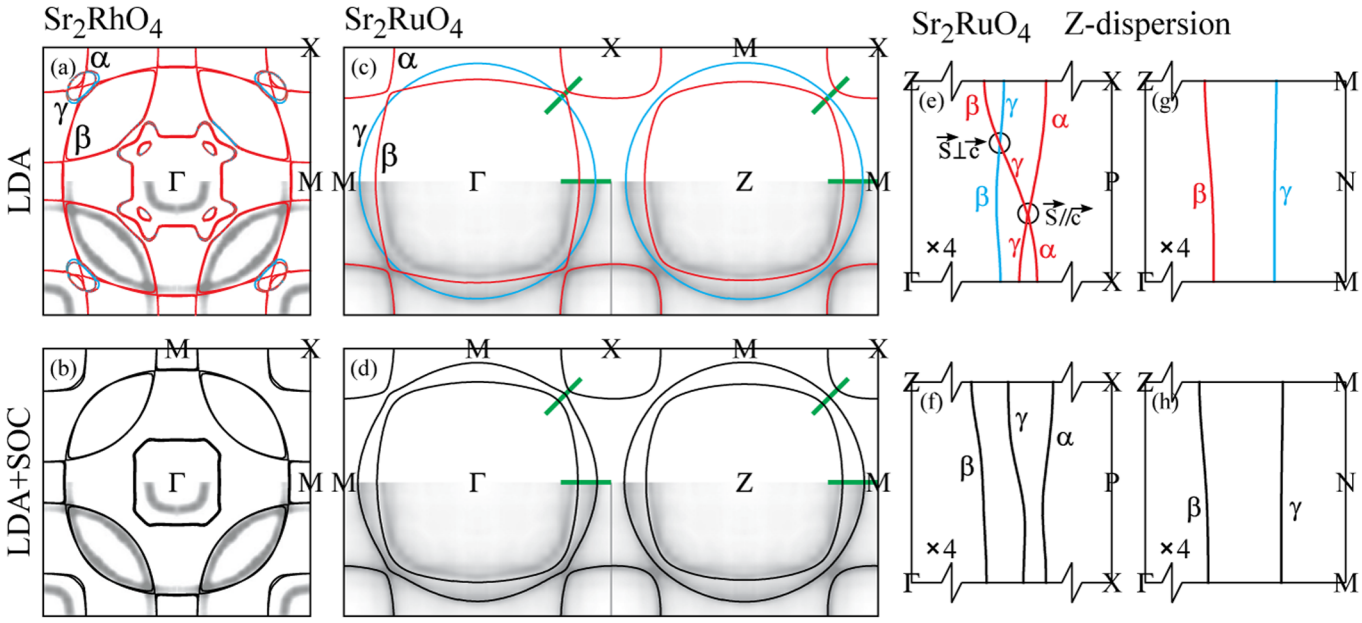

FIG. 1 (color online). (a),(b) LDA Fermi surface of Sr_2RhO_4 and (c),(d) Sr_2RuO_4; (e)–(h) k_z electronic dispersion for the Sr_2RuO_4 cuts highlighted in (c),(d) by solid green bars. Calculations were performed without SOC (top panels) and with SOC (bottom panels). The gray-scale ARPES E_F-intensity maps are here reproduced from (a),(b) Kim *et al.* [11] and (c),(d) Damascelli *et al.* [5].

Sr_2RuO_4 there are specific regions in the three-dimensional Brillouin zone where SOC does have a very large effect; this might have an important influence on the interpretation of several experimental findings, from the details of the k_z electronic dispersion [3,4] to the signatures of spin-triplet superconducting pairing [16,17].

DFT calculations were done with the code WIEN2K [18] and structural data from Ref. [19]. The results are basically independent of the radius of the muffin-tin spheres and extremely similar for local density approximation (LDA) and generalized gradient approximation, especially close to the Fermi energy. In Figs. 1(a) and 1(c), we show the Fermi surface of Sr_2RhO_4 and Sr_2RuO_4 calculated without SOC, which is in good agreement with previous theoretical results [1,2,10,11]. The Fermi surface of Sr_2RuO_4 consists of three sheets, labeled α, β, and γ. The γ sheet is mainly composed of d_{xy} orbitals and is highly two-dimensional; the α and β sheets are formed by the one-dimensional-like bands derived from d_{xz} and d_{yz} orbitals, which exhibit anticrossing behavior (i.e., mixing) along the zone diagonal. In Fig. 1(c), we present calculations for both $k_z = 0$ and π (centered around Γ and Z, respectively), which show some degree of k_z dispersion. As k_z is a difficult quantity to determine in the experiment [5], the comparison between LDA and ARPES should be attempted for various values of k_z. For $k_z = \pi$, the agreement among ARPES [5], dHvA [3] (not shown), and LDA is rather good; for $k_z = 0$, however, the crossing between γ and β sheets in LDA is experimentally not reproduced. Note that this is really a crossing and not an anticrossing, as for $k_z = 0$ the bands arising from d_{xy} and d_{xz}/d_{yz} orbitals are of different symmetry and no mixing is allowed. Also, contrary to the LDA results of Fig. 1(c), quantum oscillation experiments [3,4] indicate very little k_z modulation for the Fermi surface (smaller than 1% of the zone even for the β sheet, which exhibits the largest k_z effects).

In principle, the same discussion holds for Sr_2RhO_4; there are, however, a few complications due to structural distortions. The RhO_6 octahedra in Sr_2RhO_4 are rotated around the c axis, which results in a $\sqrt{2} \times \sqrt{2}$ doubling of the unit cell in the a-b plane and also a doubling along the c axis because of the alternation in the RhO_6 rotation direction. This leads to a doubling of all bands and Fermi sheets, as evidenced in Fig. 1(a) by the backfolding of the Fermi surface sheets with respect to the line connecting two closest M points, e.g., $(\pi, 0, 0)$ and $(0, \pi, 0)$. In addition, this distortion reduces the electronic bandwidth and allows mixing between d_{xy} and $d_{x^2-y^2}$ orbitals [11], which causes the γ sheet to almost disappear; small remaining γ pockets can be seen around the α and β sheet crossings. The agreement between LDA and experiment for the rhodate is, as shown in Fig. 1(a) and also noted in the literature [10,11], not very good (especially if compared with the beautiful agreement found for Sr_2RuO_4).

At present, there is no explanation of why LDA is able to describe Sr_2RuO_4 but fails for Sr_2RhO_4, two materials that are structurally and electronically quite similar. Here we will show that a resolution of this discrepancy can be obtained with the inclusion of SOC in LDA. As one can see in Fig. 1(b), the agreement between LDA + SOC and experiment is very satisfactory for Sr_2RhO_4: The γ sheet is now completely absent, and α and β sheets are significantly smaller (the α pocket is still somewhat larger than in the experiment, which could possibly be solved by fine-

tuning the RuO_6 distortion at the surface [11] but is beyond the point here). As for Sr_2RuO_4 [Fig. 1(d)], SOC effects are much smaller, especially for $k_z = \pi$; some improvement can be observed only for $k_z = 0$, in which case the γ and β sheet crossing becomes an anticrossing because the bands no longer have different symmetry. This point is important, as we will stress below, but first we discuss the reason why the effect of SOC for Sr_2RhO_4 seems so much stronger than for Sr_2RuO_4.

Figure 2 presents the band structure of Sr_2RuO_4 and Sr_2RhO_4 from LDA (top) and LDA + SOC (bottom). It is clear that, if the t_{2g} bands are already well separated in energy, e.g., at the M point for Sr_2RuO_4 in Fig. 2(a), SOC only mildly shifts the LDA eigenstates. A whole new energy splitting is instead induced by SOC at those momenta characterized, in LDA, by degenerate t_{2g} bands. For instance, in Fig. 2(c), the degenerate $d_{xz}^{(\uparrow,\downarrow)}$ and $d_{yz}^{(\uparrow,\downarrow)}$ LDA bands of Sr_2RuO_4 along Γ-Z are recombined into two doubly degenerate complex bands [$d_1^{\downarrow}$, $d_{-1}^{\uparrow}$ and $d_{-1}^{\downarrow}$, $d_1^{\uparrow}$, with $d_{\pm 1} = \mp\frac{1}{\sqrt{2}}(d_{xz} \pm \imath d_{yz})$], split by an energy equal to the SOC constant $\zeta = 93$ meV. Note that the latter is derived from the splitting at the Γ point, and the strong reduction with respect to the 161 meV atomic value of Ru is mainly due to the dilution effect resulting from the covalent mixing with the O-2p bands (accordingly, one also finds a SOC splitting for the O-2p derived bands around -3.8 eV due to the mixed-in Ru character, and the SOC splittings are larger at X and M points, where the covalent mixing is smaller). One might wonder, in this regard, whether the larger SOC effects in Sr_2RhO_4 might arise because of the ~20% larger atomic SOC for Rh (191 meV) as compared to Ru, originating from the somewhat less extended 4d orbitals. However, the on-site energy difference for Rh-4d and O-2p orbitals is smaller than for Ru-4d and O-2p, making Sr_2RhO_4 more covalent than Sr_2RuO_4. As a result, the *effective* SOC for the t_{2g} bands in the two compounds is about equal [Figs. 2(c) and 2(d)]; the magnitude of the atomic SOC constants is thus not the reason for the different behavior.

More clues on the magnitude of SOC effects for the two compounds come from the inspection of the Sr_2RhO_4 band dispersion in Figs. 2(b) and 2(d). The structural distortion responsible for band folding and narrowing in Sr_2RhO_4 gives rise to several nearly degenerate states close to the Fermi level [e.g., the d_{xy} band maximum at X in Fig. 2(a) is backfolded to the now equivalent Γ point, leading to the mixing with the e_g band and the appearance of two d_{xy}-derived maxima just above E_F, between Γ and X in Fig. 2(b)]. Because of the presence of weakly dispersive bands close to E_F, the SOC-induced splitting causes substantial modifications of the Fermi surface in Sr_2RhO_4 (yet in the full respect of Luttinger's theorem), such as the complete disappearance of the γ sheet [Fig. 2(f)]. On the contrary, in the case of Sr_2RuO_4 in the very same k-space region [Fig. 2(e)], the energy shift from SOC does not translate in large changes in k because of the steep band dispersion. It is therefore the interplay between SOC and band filling (i.e., the presence, or lack thereof, of weakly dispersive degenerate states close to the chemical potential), which determines the more dramatic Fermi surface changes for Sr_2RhO_4 in LDA + SOC. Larger effects should be expected for Sr_2RuO_4 upon increasing the electron filling; this has indeed been observed in the case of $Sr_{2-y}La_yRuO_4$ [20], in which the γ-sheet topological transition detected for $y \gtrsim 0.20$ is well accounted for by LDA + SOC (not shown).

In the following, we will focus on some aspects of the LDA + SOC results which, beyond the detailed analysis of the Fermi surface, promise to have profound implications for the physical properties of Sr_2RuO_4. We have already noted, in relation to Fig. 1(c), that for $k_z = 0$ the LDA calculations display the crossing of γ and β sheets at eight momenta symmetrically located with respect to the Γ-X lines. As SOC is not a small perturbation at highly degenerate k points in LDA, to understand the impact of SOC on the low-energy physics we have to follow this degeneracy as a function of k_z. In Figs. 1(e) and 1(g), we plot the k_z modulation of the LDA Fermi sheets in the Γ-X-Z and Γ-M-Z planes. The k-space loci of γ and β sheet degeneracy in LDA defines an elliptical contour centered around the Γ-X line, crossing the $k_z = 0$ plane at $(k_x, k_y) = (0.28\pi, 0.34\pi)$ and $(0.34\pi, 0.28\pi)$ as indicated in Fig. 1(c) and crossing the Γ-X-Z plane at $k_z = 0.68\pi$. This is a degeneracy between the d_{xy} orbital and a linear combination of d_{xz} and d_{yz} orbitals; there is also a further

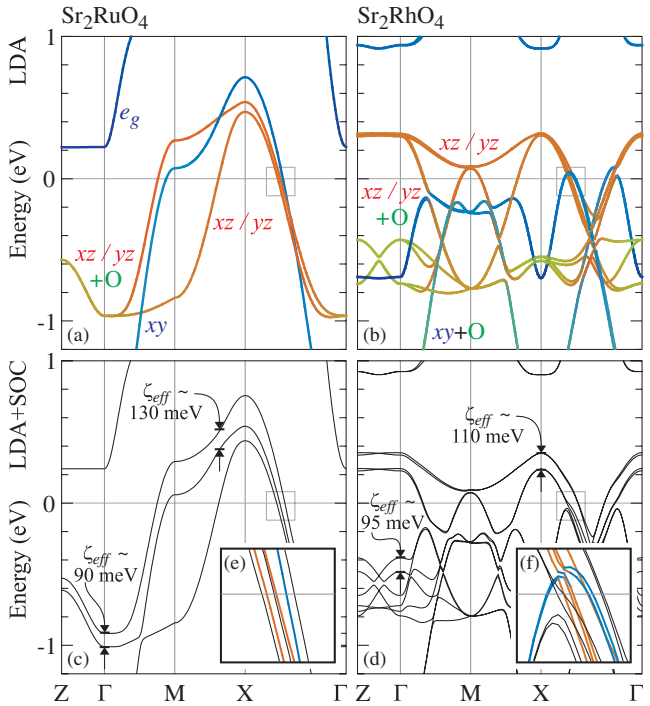

FIG. 2 (color online). LDA (top) and LDA + SOC (bottom) band dispersion of Sr_2RuO_4 (left) and Sr_2RhO_4 (right). (e),(f) Enlarged view of the marked E_F regions in (c),(d).

degeneracy at $(k_x, k_y, k_z) = (0.34\pi, 0.34\pi, 0.33\pi)$ between the d_{xz} and d_{yz} orbitals [Fig. 1(e)]. In addition to lifting the degeneracy of the LDA Fermi surfaces [Fig. 1(f)], the inclusion of SOC reduces to more realistic values the k_z modulation of each individual Fermi surface sheet, which in LDA is much larger than observed in quantum oscillation experiments [3,4]. Note, in this regard, that the rather localized bulging of the Fermi surfaces in LDA + SOC, such as, e.g., along the zone diagonal for $k_z = 0$ for the γ sheet, might require the inclusion of higher-order cylindrical harmonics than usually considered in the quantum oscillation analysis [3,4].

Perhaps more important, SOC is responsible for the three-dimensional k dependence of the wave function spin and orbital character, along the Fermi surface. For instance, the character of the γ sheet is no longer pure d_{xy}; instead, for $k_x = k_y$ and $|k_z| < 0.68\pi$, it is mainly a linear combination of d_{xz} and d_{yz}. This not only influences the hopping parameters, it also has a large effect on the spin anisotropy. At $(0.34\pi, 0.34\pi, 0.33\pi)$, SOC recombines the degenerate $d_{xz}^{(\uparrow,\downarrow)}$ and $d_{yz}^{(\uparrow,\downarrow)}$ orbitals into the two doubly degenerate $d_1^{\downarrow}$, $d_{-1}^{\uparrow}$ and $d_{-1}^{\downarrow}$, $d_1^{\uparrow}$ complex orbitals. These new eigenstates have a spin moment in the z direction and a zero expectation value for x and y spin components. This follows from $s_x = \frac{1}{2}(s^+ + s^-)$ and $\langle d_1^{\downarrow}|s^-|d_{-1}^{\uparrow}\rangle = 0$, as the orbitals are orthogonal to each other, and analogous relations for s^+ and s_y. Thus, at $(0.34\pi, 0.34\pi, 0.33\pi)$ the spins on the γ and α sheets point along the c axis, as indicated in Fig. 1(e). Similar arguments can be made if the d_{xy} and d_{xz} or d_{yz} orbitals are degenerate. By cyclic permutation of coordinates, it can be shown that this leads to a spin direction in the a-b plane [Fig. 1(e)], along the whole elliptical LDA-degeneracy contour between γ and β sheets discussed above. Note that this k-dependent noncollinear spin anisotropy cannot easily be seen in the bulk magnetic susceptibility, which measures an average over all k points. It has, however, severe implications for all k-dependent properties of Sr_2RuO_4.

Our study shows that, when describing experiments on Sr_2RuO_4 and Sr_2RhO_4, it is crucial to start from accurate *ab initio* band-structure calculations including SOC. One should be careful about a phenomenological modeling of the electronic structure. For instance, a simple tight-binding fit to the experimentally determined Fermi surface of Sr_2RuO_4 leads to nondegenerate bands at the Fermi energy; adding SOC, starting from such a scenario, would introduce only a small perturbation. SOC is, however, not a small perturbation for metals if (nearly) degenerate bands cross or are close to the Fermi energy, which happens for Sr_2RhO_4 in extended portions of the Brillouin zone and for Sr_2RuO_4 at some momenta. This has important implications—macroscopic in the case of Sr_2RhO_4—for fundamental properties such as the detailed shape and orbital character of the Fermi surface sheets, as well as the amount of k_z dispersion. For example, SOC is responsible for a significant reduction of the effective three-dimensionality in Sr_2RuO_4, which is consistent with the dHvA results [3]. Also, even in the overall less dramatic case of Sr_2RuO_4, SOC leads to a spin anisotropy and noncollinear behavior in several k-space regions, with the spin precession direction varying with k according to the orbital character of the LDA + SOC eigenstates. This k-dependent orientation of the expectation value of the spin calculated on the LDA + SOC eigenstates, which reminds us of Rashba coupling, could be a very important ingredient in describing the superconducting state of Sr_2RuO_4 and should be investigated further. Since all Fermi surface degeneracies are lifted in LDA + SOC and the k-dependent energy splittings are much larger then the superconducting pairing energy, the SOC-induced spin anisotropy in concert with orbital mixing should directly affect the orbital and spin angular momentum of the Cooper pairs. In fact, singlet and triplet states could be strongly mixed, blurring the distinction between spin-singlet and spin-triplet pairing [13] and with it the simple interpretation of time-reversal symmetry-breaking experiments [16,17].

This work was supported by the Alfred P. Sloan Foundation (A. D.), CRC and CIFAR Quantum Materials Programs (A. D. and G. A. S.), NSERC, CFI, BCSI, the Deutsche Forschungsgemeinschaft (DFG) through SFB 608, and NSF under Grant No. PHY05-51164.

[1] T. Oguchi, Phys. Rev. B **51**, 1385 (1995).
[2] D. J. Singh, Phys. Rev. B **52**, 1358 (1995).
[3] C. Bergemann *et al.*, Phys. Rev. Lett. **84**, 2662 (2000).
[4] D. Forsythe *et al.*, Phys. Rev. Lett. **89**, 166402 (2002).
[5] A. Damascelli *et al.*, Phys. Rev. Lett. **85**, 5194 (2000).
[6] A. Sekiyama *et al.*, Phys. Rev. B **70**, 060506 (2004).
[7] N. Hiraoka *et al.*, Phys. Rev. B **74**, 100501(R) (2006).
[8] N. J. C. Ingle, *et al.*, Phys. Rev. B **72**, 205114 (2005).
[9] S. Nakatsuji and Y. Maeno, Phys. Rev. Lett. **84**, 2666 (2000).
[10] F. Baumberger *et al.*, Phys. Rev. Lett. **96**, 246402 (2006).
[11] B. J. Kim *et al.*, Phys. Rev. Lett. **97**, 106401 (2006).
[12] R. S. Perry *et al.*, New J. Phys. **8**, 175 (2006).
[13] M. Sigrist *et al.*, Physica (Amsterdam) **317C–318C**, 134 (1999).
[14] T. Mizokawa *et al.*, Phys. Rev. Lett. **87**, 077202 (2001).
[15] A. Earnshaw *et al.*, J. Chem. Soc. **601**, 3132 (1961). The SOC Hamiltonian is $\sum_i \zeta l_i \cdot s_i$, where l_i (s_i) is the orbital (spin) angular-momentum operator for the ith electron and the sum runs over all i electrons.
[16] G. Luke *et al.*, Nature (London) **394**, 558 (1998).
[17] J. Xia *et al.*, Phys. Rev. Lett. **97**, 167002 (2006).
[18] P. Blaha *et al.*, in *An Augmented Plane Wave and Local Orbitals Program for Calculating Crystal Properties*, edited by K. Schwarz (Technical University of Wien, Vienna, 2001).
[19] T. Vogt and D. J Buttrey, Phys. Rev. B **52**, R9843 (1995); J. Solid State Chem. **123**, 186 (1996).
[20] K. M. Shen *et al.*, Phys. Rev. Lett. **99**, 187001 (2007).